

Proving the Uplink Array for Radar Observations

Victor Vilnrotter,* Joseph Jao,† Jon Giorgini,† Dennis Lee,* Philip Tsao‡

ABSTRACT. — Due to the monolithic antenna design of the Goldstone Solar System Radar (GSSR), the transmitter power of the GSSR can only be increased by installing higher power klystrons, which are likely reaching their limit around 250 kW. These klystrons have not been very reliable in the past. By contrast, the Phased Array Transmitter concept is a distributed system that coherently combines signals from multiple 34 m antennas at the target, producing a reliable high-power radar system that can serve as viable backup to the GSSR. Our goal is to demonstrate a high-power wideband Phased Array Transmitter concept to meet requirements for planetary science, planetary defense, and cislunar space domain awareness by configuring two of the Deep Space Network’s 34 m antennas, namely Deep Space Station 13 (DSS-13) and DSS-26, as an Uplink Array Radar system.

I. Introduction

As NASA returns to the Moon, there is increased emphasis on tracking spacecraft in cislunar space. The Goldstone Solar System Radar (GSSR) on the Goldstone 70 m antenna has demonstrated capability to detect and track spacecraft around the Moon, having detected both the Lunar Reconnaissance Orbiter and the Chandrayaan-1 spacecraft. In addition, the Deep Space Network (DSN) has developed an X-band (nominally 7.2 GHz) Uplink Array capability, initially intended for spacecraft commanding, at the Apollo Station consisting of Deep Space Stations 24, 25, and 26 (DSS-24, DSS-25, DSS-26). The Uplink Array is a distributed phased array system that coherently combines signals from multiple 34 m antennas at the target to produce a high-power system. The Uplink Array offers two potential advantages relative to the GSSR. First, because it uses 34 m antennas, the effective field of view is approximately four times larger than that of the 70 m antenna. Second, the GSSR depends on two ultra-high-power klystrons that are challenging to design and maintain; because the DSN Uplink Array uses multiple antennas, each equipped with lower power and more reliable klystrons, it is, in principle, more robust than the GSSR.

It is well known that an Uplink Array consisting of N identical antennas generates N^2 times greater Effective Isotropic Radiated Power (EIRP) than a single antenna, because with

* Tracking Systems and Application Section.

† Communications Architectures and Research Section.

‡ Formerly Tracking Systems and Application Section.

perfect phasing, the field amplitudes at the target add coherently, hence the power increases by a factor of N^2 in the far-field [1, 2].

The current Goldstone Uplink Array consists of three DSN 34 m antennas at the Apollo Station shown in Figure 1, DSS-24/25/26, equipped with 20 kW, 20 kW, 80 kW output power, respectively. Long term, the DSN plans to deploy four 34 m antennas to each of the three complexes (Goldstone, Canberra, Madrid), and there is the potential to add additional antennas to each complex or to provide all antennas with 80 kW klystrons, or both. As an illustration of the potential of Uplink Array Radars, four 34 m antennas, for example, each equipped with 80 kW antennas, would be equivalent to a 320 kW transmitter on a 70 m antenna; meanwhile, five 34 m antennas with 80 kW would equal the EIRP of a 70 m antenna with a 500 kW transmitter.

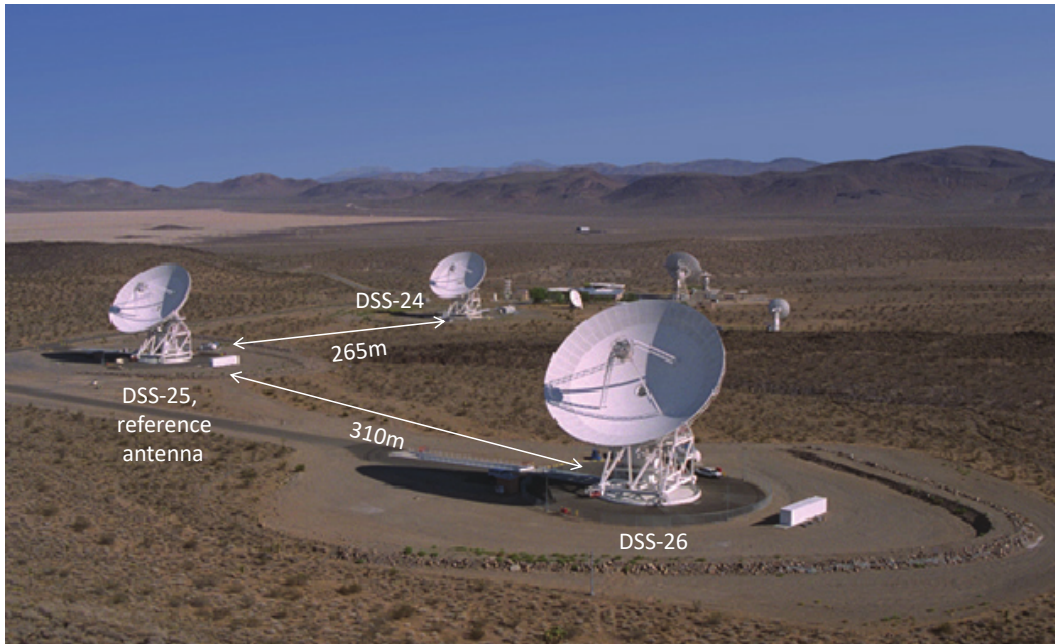


Figure 1. The three antennas of the DSN Uplink Array, DSS-24/25/26, at the Apollo Station.

The two-element Uplink Array Radar development effort employs the 34 m DSS-26 at the Apollo Station and the 34 m research antenna DSS-13 at the Venus Station as the radar transmitters, both equipped with 80 kW X-band transmitters, operating at the DSN uplink frequency of 7150 MHz. The DSS-13 antenna is shown in Figure 2. The operational DSN receivers operate at the transponded spacecraft downlink frequency of roughly 8400 MHz; hence they are not suitable for receiving the nominal 7150 MHz radar echoes.

However, the 34 m DSS-28 Goldstone Apple Valley Radio Telescope (GAVRT) antenna shown in Figure 3 was upgraded to receive 7150 MHz DSN uplink signals. In this application, the downlink signals are not turned around at a different frequency as with NASA spacecraft, but rather they bounce off the target and return to the receiver at the same nominal uplink frequency, plus a small Doppler offset due to relative velocity between the transmitter and the target. The DSS-28 antenna is located roughly 1.5 km from the Venus site.



Figure 2. The DSS-13 research antenna at the Venus Site, equipped with an 80 kW X-band transmitter.



Figure 3. The 34 m GAVRT antenna at DSS-28 that received the radar echoes from the Moon in bistatic configuration.

The relative locations of the DSS-13 and DSS-26 antennas forming the long transmitter baseline, as well the location of the DSS-28 receiver, are shown in Figure 4, illustrating the key difference between the two- and three-element Apollo Uplink Array demonstrated previously with 20 kW transmitters on short, approximately 265–310 m baselines, and the new Uplink Array Radar system with 80 kW transmitters located on a 12 km baseline, resulting in much narrower array fringes with spacing inversely proportional to the baseline.



Figure 4. Geometry of Apollo Station, DSS-13, and DSS-28 at the Goldstone Deep Space Communications Complex.

Following equipment installation and initial tests, experiments were planned to demonstrate single-antenna Doppler-delay imaging of the Tycho region on the Moon using either DSS-13 as the transmitting antenna or one of the Apollo antennas, DSS-24/25/26. These radar imaging tests were intended to demonstrate nominal antenna operation, signal distribution from DSS-28 to the DSS-13 control room, effectiveness of the frequency and delay predicts, and nominal functioning of the signal-processing equipment and algorithms.

II. Upgrading and Installing Uplink Array and GSSR Equipment

In December 2019, the Uplink Array Radar team traveled to the Goldstone Deep Space Communications Complex (GDSCC) at Fort Irwin, CA, to evaluate the status of the inherited Uplink Array and new GSSR equipment, including the Phase Comparator Assembly (PCA) previously used to align the phase of Apollo antennas DSS-24/25/26, configured as two- and three-antenna Uplink Arrays.

A. Evaluating Status of Uplink Array and GSSR Equipment at Goldstone

First, the Uplink Array Radar team inspected existing and upgraded equipment at the Venus site, including the 80 kW transmitter, the coupler designed to pick off the return signal from the high-power transmitter, and the upgraded X-band-to-320 MHz intermediate frequency (IF) downconverter assembly newly installed into a full rack in the DSS-13 pedestal room (see Figure 5). The 80 kW transmitter was turned ON, and the coupled carrier was observed on a spectrum analyzer, validating nominal operation of the 80 kW transmitter assembly at DSS-13.



Figure 5. X-band (7150 MHz) to 320 MHz IF downconverter assembly in the DSS-13 antenna's pedestal room.

Next, the team drove to Signal Processing Center 10 (SPC-10), located the DSS-13 320 MHz IF output on the IF panel, and observed the unmodulated 320 MHz IF signal both on a spectrum analyzer and on a wideband oscilloscope. Signal quality was nominally the same as at the Venus site control room, implying no significant degradation in the transit over the fiber optic channel. Visual observation of the 320 MHz IF signal indicated roughly 1/20th radian root-mean-squared (rms) phase error, which would be more than adequate for high-quality phase-coherent Uplink Array Radar combining.

After the seismic upgrade at SPC-10, the Uplink Array Radar PCA and its support equipment were located at SPC-10, removed from the inherited half-rack, and are now installed in a seismically isolated full rack. It was found that the electric power strip on the new full rack could not be connected because official approval was needed to power up the PCA due to restrictions on power consumption. After returning to Jet Propulsion Laboratory, a formal request was submitted, and approval was obtained to power up the PCA for future operations.

B. Upgrading the DSS-28 Antenna for 7150 MHz Reception

The DSS-28 GAVRT antenna was repaired and configured for Uplink Array Radar applications to be used as the receiver for the 7150 MHz DSN uplink frequency in the Uplink Array Radar demonstrations (see Figure 6). The received radar signal is down-



Figure 6. DSS-28 receiving equipment upgraded at GDSCC in order to receive 7150 MHz echoes from the Tycho region on the Moon.

converted to 320 MHz IF and relayed from DSS-28 to the DSS-13 control room, where it is processed to obtain Doppler-delay images of the Tycho region with the GSSR Signal Processing Assembly. The DSS-28 antenna pointing is controlled from the GAVRT control center in Apple Valley, CA, using custom pointing predicts generated specifically for Uplink Array Radar demonstrations.

C. Installation and Fine-Tuning of GSSR Equipment at SPC-10 and DSS-13

The Uplink Array Radar demonstrations require the use of GSSR radar equipment, including the recently developed GSSR Waveform Generators (WFGs) at DSS-13 and SPC-10. The two upgraded WFG assemblies were installed at SPC-10 and the DSS-13 control room, and were tested to validate nominal operation.

The WFG assemblies installed at SPC-10 and at the Venus site generate the pseudo-noise (PN) code modulation required for Doppler-delay imaging of the radar target. At SPC-10, the baseband analog output of the WFG is connected to the port labeled “Test Mod in” of the operational Uplink Signal Generator (USG) corresponding to the scheduled Apollo antenna in SPC-10 (nominally, DSS-26 with 80 kW transmitter, but DSS-24/25 with 20 kW transmitters can also be used for experimental demonstrations), where it is phase-modulated onto the 7150 MHz uplink carrier. A block diagram of the USG, with the input port identified is shown in Figure 7 [4], and a picture of the WFG assembly is shown in Figure 8.

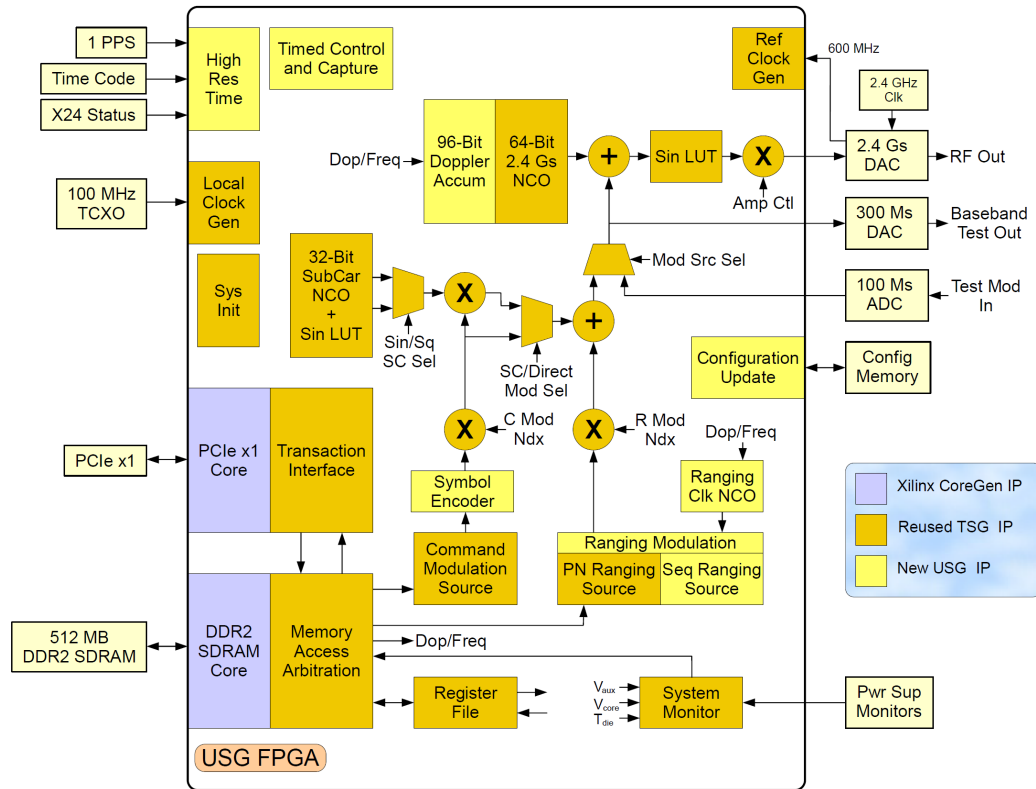


Figure 7. USG block diagram, showing the WFG signal input port [4].

The division of uplink signal power between modulation and residual carrier is determined by the modulation index m , which varies between 0 and $\pi/2$ radians: with $m = \pi/2$, the residual carrier is completely suppressed and all of the signal power is contained in the modulation; with $m = 0$, the modulation is fully suppressed with all the power in the carrier.

For Doppler-delay imaging of radar targets, the modulation power should be maximized for best image quality, because the residual carrier contains no useful information. The modulation index is determined by the amplitude of the baseband PN-code input to the Test Mod port; hence it can be optimized by observing the spectrum of the return signal at SPC-10, and the WFG output signal amplitude can be adjusted to minimize the residual carrier.

Minimization of the residual carrier was carried out for all three Apollo antennas, demonstrating that the residual carrier can be fully suppressed in the DSS-24 and DSS-25 transmitted signals but only partially suppressed in the DSS-26 signal. This problem remains to be examined and corrected in the future; however, initial indications are that the minimized residual carrier does not cause serious degradation in the DSS-26 Doppler-delay images.

III. Differential Frequency and Doppler Predicts for DSS-13

Time-varying relative motion between the transmitters and the target result in signals that arrive at the target with a time-varying Doppler frequency. In order to produce stable interference fringes at the target, it is therefore necessary to pre-compensate the transmitted signals on the ground to ensure that they arrive at the target with the same frequency and constant phase. This is accomplished by predicting the Doppler frequency at the target for each antenna using the known link geometry and applying a pre-compensating frequency before the signal is transmitted towards the target [3]. However, the operational transmitters of the DSN employ linear frequency ramps between pre-computed points typically separated by 25 seconds, with a maximum of 500 points per predict file, whereas the GSSR WFG computes a complex phase for each sample in real time using 15th-order Chebyshev coefficients, which could be spaced in time by as little as 5 nanoseconds. These two predict formats are not compatible, and hence it was decided to transmit a constant frequency uplink carrier of exactly 7150 MHz from the Apollo antennas. The time-varying Doppler frequency can be compensated at the target by applying “differential predicts” to the DSS-13 transmitter at the high-frequency sample rate to ensure that the signals from the two antennas (DSS-13 and one of the Apollo antennas) arrive at the target with the same frequency and constant phase. A computational approach was developed using data in standard GSSR-format radar predicts to derive the differential DSS-13 transmit time and frequency necessary to produce the same apparent frequency from the Apollo antennas seen at the target echo reflection point, enabling the generation of interference fringes.



Figure 8. Picture of the GSSR WFG installed at DSS-13 and SPC-10.

A conceptual diagram of the Earth-Moon geometry for two-antenna array fringe generation at the crater Tycho is shown in Figure 9. A station transmitting at a fixed frequency results in a time-varying frequency at the target due to the apparent expansion or compression of the electromagnetic wave if there is relative motion between the transmitter and target. This is known as “Doppler frequency shift.” To maximize interference fringes at the target, it is necessary—though not sufficient—to vary a second station's transmitter frequency so a second signal arrives at the target at the same apparent frequency as the signal from Station 1. In general, this second transmitter station will have a different relative motion with respect to the target than Station 1 and, thus, a different Doppler frequency shift due to its different location on a rotating and translating surface relative to the target, which is also moving.

It is, therefore, necessary to solve for the time-varying transmitter frequency required for Station 2 to bring about a matching frequency at the target, with subsequent reception of the interference-fringed echo at a third station. The conditions for this three-way Doppler model can be summarized as follows:

1. Station 1 transmits at a fixed uplink frequency (e.g., 7150 MHz).
2. Station 2 transmits at a time-varying uplink frequency to be determined from the link geometry.

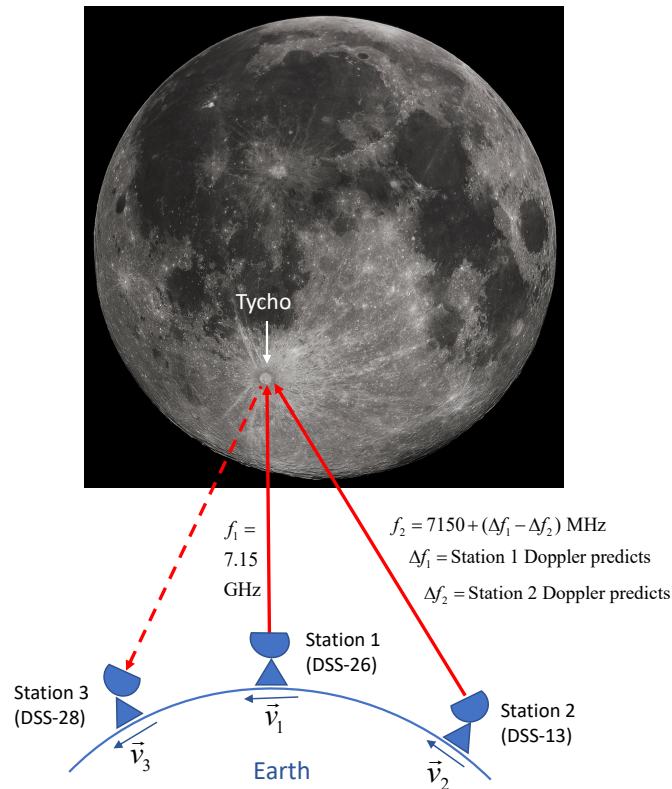


Figure 9. Uplink Array Radar geometry and key equations required for differential Doppler and delay compensation by the DSS-13 transmitter, with the Apollo antenna transmitting a constant frequency signal at 7150 MHz.

3. Carriers for both transmitters must arrive at the target point at the same Doppler-shifted apparent frequency to maximize interference.
4. Station 3 receives the interference-fringed echo from the target with a residual Doppler frequency, which can be compensated in post-processing.

For the following detailed derivation of the required frequency predicts, we define the following quantities for the transmitters and receiver:

- f_r = Received frequency, Hz
- f_t = Transmitted frequency, Hz
- f_b = Base reference frequency (e.g., 7150 MHz)
- τ_x = Transmission time of a given signal at a transmitter
- τ_r = Reception time of signal at a receiver

For receiver Station 3, where times are referenced to reception time τ_r , we also define the following quantities in terms of the basic definitions above:

- $\Delta\tau_r = \tau_r - \tau_x$ (Round-trip delay, seconds)
- $\Delta f_{rt} = f_r(\tau_r) - f_t(\tau_x)$ (Doppler frequency shift, Hz)
- $\Delta f_{rb} = f_r(\tau_r) - f_b$ (Differential Doppler, Hz)

Because these derived values are known and available from standard, fixed-frequency bistatic GSSR transmitter predicts, a computational approach was developed to use data available in those prediction files to derive the Station 2 transmit time and frequency necessary to match the apparent frequency of Station 1 seen at the target echo reflection point, and enable maximum interference-fringe production.

Expanding the difference yields $\Delta f_{rb} - \Delta f_{rt} = [f_r(\tau_r) - f_b] - [f_r(\tau_r) - f_t(\tau_x)]$ and after canceling terms, rearranging, and substituting, we obtain

$$f_t(\tau_x) = 7150 \times 10^6 + (\Delta f_{rb} - \Delta f_{rt}) \text{ Hz} . \quad (1)$$

Writing out variations of Equation (1) for the two specific transmitters denoted by subscripts,

Station 1 (fixed frequency transmitter): The Apollo Station antennas operate with a fixed frequency of 7150 MHz; hence the transmitter frequency at Station 1 can be written as

$$f_t(\tau_x)_{_1} = 7150 \times 10^6 + (\Delta f_{rb_{_1}} - \Delta f_{rt_{_1}}) \text{ Hz} .$$

Noting that $f_r(\tau_x)_{-1}$ is 7150 MHz for the fixed frequency transmitter by definition, this reduces to

$$\Delta f_{rb_{-1}} = \Delta f_{rt_{-1}}. \quad (2)$$

$\Delta f_{rb_{-1}}$ and $\Delta f_{rt_{-1}}$ are known, being given in the receiver section of standard GSSR fixed-frequency transmitter predicts.

Station 2 (variable frequency transmitter): Similarly,

$$f_t(\tau_x)_{-2} = 7150 \times 10^6 + (\Delta f_{rb_{-2}} - \Delta f_{rt_{-2}}) \text{ Hz}. \quad (3)$$

$\Delta f_{rt_{-2}}$ is known, being given in the receiver section of standard GSSR fixed-frequency transmitter predicts. This leaves $\Delta f_{rb_{-2}}$ as the remaining unknown needed to specify the desired $f_t(\tau_x)_{-2}$ for the variable frequency transmit case.

Subtracting the two differential Dopplers,

$$\Delta f_{rb_{-1}} - \Delta f_{rb_{-2}} = f_r(\tau_r)_{-1} - f_b - f_r(\tau_r)_{-2} + f_b.$$

The constants f_b cancel, simplifying to:

$$\Delta f_{rb_{-1}} - \Delta f_{rb_{-2}} = f_r(\tau_r)_{-1} - f_r(\tau_r)_{-2}.$$

Because the signal path from the interference-reflection point at the target to the receiver (down-leg) is the same for both carrier paths, original condition #3 (“same frequency at interference point”) means the received frequency at Station 3 (after an identical down-leg) will also be the same for the two carrier paths:

$$\Delta f_{rb_{-1}} - \Delta f_{rb_{-2}} = f_r(\tau_r)_{-1} - f_r(\tau_r)_{-2} = 0.$$

Therefore, at receiver Station 3

$$\Delta f_{rb_{-1}} = \Delta f_{rb_{-2}}.$$

With $\Delta f_{rb_{-2}}$ now in terms of something available from the fixed-frequency transmit predicts, Equation (3) can be rewritten:

$$f_t(\tau_x)_{-2} = 7150 \times 10^6 + (\Delta f_{rb_{-1}} - \Delta f_{rt_{-2}}) \text{ Hz}. \quad (4a)$$

Because Station 1 is transmitting at a fixed frequency (e.g., 7150 MHz), Equation (2) can be substituted to obtain an equivalent expression,

$$f_i(\tau_x)_{-2} = 7150 \times 10^6 + (\Delta f_{r_{-1}} - \Delta f_{r_{-2}}) \text{ Hz} . \quad (4b)$$

If computing Doppler by differentiating round-trip delay Chebyshev polynomials, this can also be written as:

$$f_i(\tau_x)_{-2} = 7150 \times 10^6 + \left(d(\Delta \tau_{r_{-1}}) / dt - d(\Delta \tau_{r_{-2}}) / dt \right) \times f_b \text{ Hz} . \quad (4c)$$

With Equation (4) giving the required Station 2 transmit frequency at earlier time τ_x for reception at time τ_r , it is necessary to compute the required transmit time τ_x for this frequency.

From the original definitions, transmit time τ_x for $f_i(\tau_x)_{-2}$ to meet the far-field fringe requirement is:

$$\tau_x = \tau_r - \Delta \tau_{r_{-2}} \text{ sec} . \quad (5)$$

$\Delta \tau_{r_{-2}}$ is available in the receiver section of standard bistatic GSSR radar predicts for Station 2.

Operationally, fringe production can therefore be accomplished given two sets of standard bistatic GSSR predicts. One set provides transmitter predicts for Station 1 transmitting at a fixed frequency with receiver predicts for Station 3. The other set provides transmitter predicts for Station 2, also transmitting at a fixed frequency and with receiver predicts for Station 3.

Software then pre-processes the receiver sections from these two input sets of standard fixed-frequency predicts at times τ_r and produces a new variable-frequency transmitter model $f_i(\tau_x)$ for Station 2 at any time τ_x , using Equations (4a, b, c) and (5), to maximize signal interference and fringe production at the target point.

IV. Single-Antenna Doppler-Delay Imaging of the Tycho Region

After installation and testing of the GSSR equipment at SPC-10 and DSS-13, and after fine-tuning of the WFG outputs to minimize the residual carrier in the uplink signals from the Apollo antennas, antenna schedule reports were obtained from DSN Scheduling and used to identify Apollo antenna availability. Due to the relative complexity of a lunar Doppler-delay imaging experiment—including boresighting the DSS-13 antenna to refine pointing, calibrating the high-power transmitters, and analyzing the real-time data—tracks of at least 6 hours duration are preferred. DSS-13 and DSS-28 also have to be coordinated, but

permission can usually be obtained for these antennas from GAVRT and DSS-13 scheduling.

A block diagram of the DSS-13/26/28 Uplink Array Radar demonstration system is shown in Figure 10. DSS-13 and DSS-26 (or another Apollo antenna such as DSS-24/25 scheduled for these preliminary concept demonstrations) are pointed at the target crater Tycho on the Moon, illuminating it with differentially compensated 11th-order Pseudo-Noise (PN-11) code modulated X-band carriers and the radar echo received at DSS-28. The received signals are down-converted to 320 MHz IF and sent to the DSS-13 control room for processing. The IF signals are further down-converted to complex baseband and processed to extract Doppler-delay images of the Tycho region.

Two Moon-bounce radar tracks were scheduled in February 2020, on Day of Year 35 (DOY-035) and DOY-037. The DSN antennas DSS-26 and DSS-13 were scheduled for these tracks, both equipped with 80 kW X-band transmitters. The DSS-28 GAVRT antenna received the radar echoes, operated from the GAVRT control center in Apple Valley. These initial “Moon-bounce” experiments were aimed at imaging the Tycho region in preparation for phasing up the Uplink Array Radar system by centering the brightest fringe over the central peak of the crater Tycho.

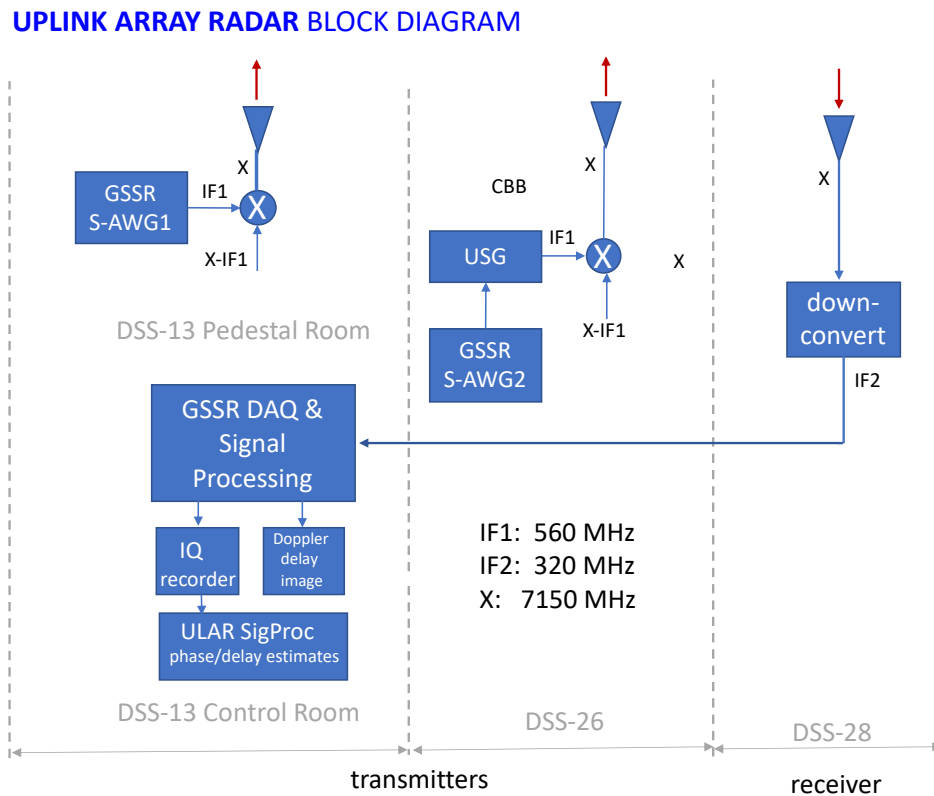


Figure 10. Block diagram of the Uplink Array Radar system for the DSS-13/26/28 link, including signal processing at DSS-13.

A. DSS-13/28 Bistatic Radar Link

It was observed on DOY-035 that shortly before lunar transit, the DSS-13 transmitting antenna was pointing in the general direction of the DSS-28 receiving antenna, causing a strong leakage signal that enters the DSS-28 receiver through the sidelobes. This was likely due to the line-of-sight transmission from DSS-13 to DSS-28. An example of the PN-code modulated signal is shown in Figure 11a. It can be seen that both the in-phase (I, blue) and quadrature (Q, red) components are saturated at roughly ± 128 quantization levels in the digital domain with 8-bit quantization. The sampling rate was set to 8 Msps on both days, DOY-035 and DOY-037, generating 40 samples per 5-microsecond PN chip. An unexpected advantage of the strong multipath signal is that the reference PN-code can be obtained directly from the signal itself by taking the sign of the stronger of the I and Q components, even if the PN-code generator polynomial taps and initial conditions are not readily available.

The zoomed-in version in Figure 11b shows an image of the PN-code modulated carrier, demonstrating severe saturation in the Q channel (which rotates into the I channel, as shown in Figure 11a). This saturation problem was eliminated in subsequent tracks by attenuating the signal to better match the voltage range of the analog-to-digital converters.

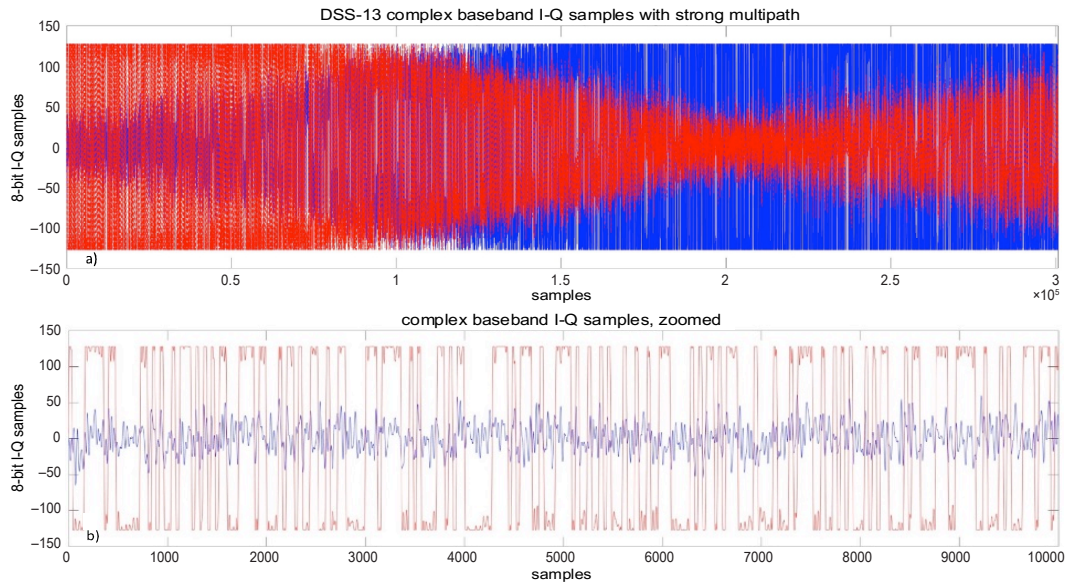


Figure 11. Baseband signals with strong multipath (DSS-13/28 link): a) long time interval showing phase rotation in the I-Q samples; b) short time interval version at the start of the data set, showing the clipped PN-code in the Q component (red).

B. DSS-26/28 Bistatic Radar Link

It was observed on DOY-035 that the DSS-26 modulated signal contained a large residual carrier; therefore, a second attempt was made on DOY-037 to minimize the residual carrier by readjusting the amplitude of the WFG output signal, which was input to the DSN USG. This is the only option for adjusting the residual carrier with the USG when the test port is used to input an external waveform. However, even at the best amplitude setting, a relatively large residual carrier remained in the transmitted spectrum (approximately 20 dB

above the modulation peak). Although the residual carrier represents lost modulation power, it did not seem to impact the quality of the Doppler-delay images obtained in subsequent tracks.

V. Doppler-Delay Signal Processing

The underlying concept of the Doppler-delay signal processing algorithms designed to post-process the complex baseband data is best explained using conventional time-domain analysis, although the GSSR receiver uses an equivalent but more efficient frequency domain algorithm to generate images in near real-time. The transmitted PN sequences are reflected from the target and bounce back to the radar receiver in the form of scintillating echoes, which are then compressed into narrow pulses via cross-correlating with a noiseless local copy of the PN-code, a segment of which is shown in Figure 12.

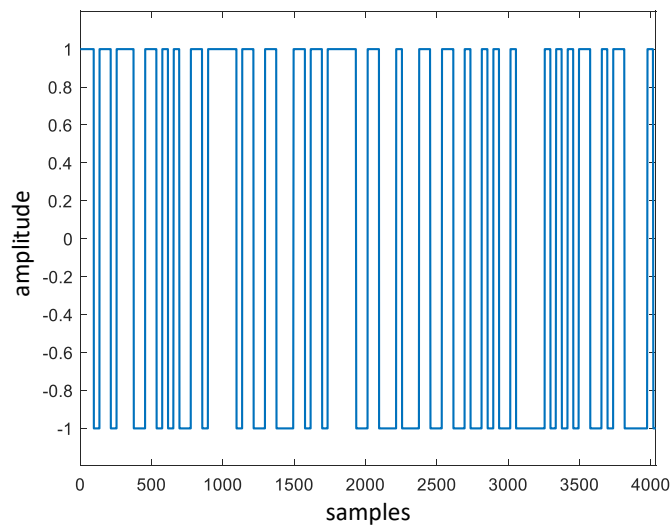


Figure 12. Segment of reference PN-code used on DOY-037 to cross-correlate with the received fluctuating and noise-corrupted radar echo.

The cross-correlation operation yields narrow single-chip pulses corresponding to reflections with different delays from the target region. In this example from DOY-037, the PN-code is 2047 chips long, and there are 40 samples per chip; hence the pulse repetition period (PRP) is 81880 samples, as shown in Figure 13.

The Doppler dimension in the image can be obtained by taking the Fast Fourier Transform (FFT) of a sequence of complex values from each delay in the compressed pulse-train, as shown in Figure 13 with the red arrows at multiples of 81880 samples for this example.

The cross-correlation operation can also be implemented equivalently and more efficiently using the FFT, simply by multiplying the FFTs of the received and local data sequences, and inverse-transforming the result. The DCAR uses this FFT approach to obtain near real-time Doppler-delay images, examples of which are shown in Figure 14.

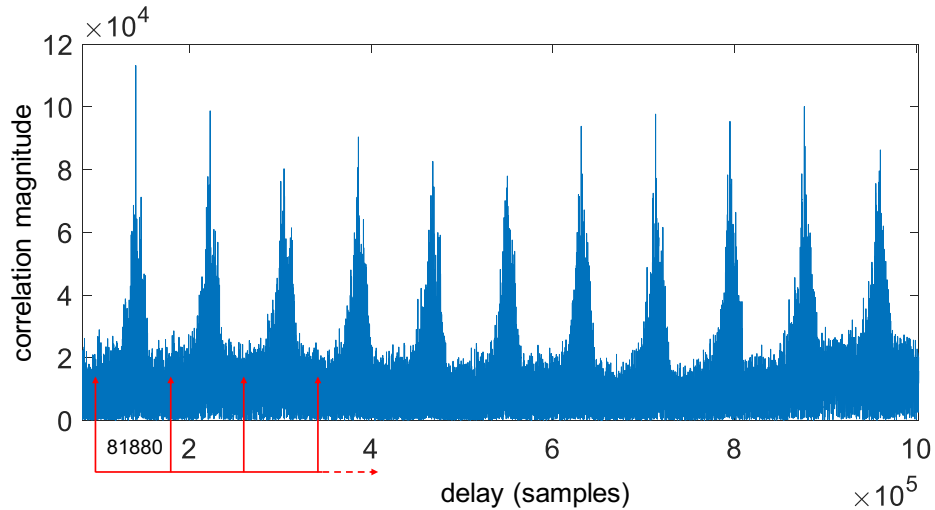


Figure 13. Correlator output showing the sequence of compressed PN-code pulses reflected from lunar features with different delays.

A. DCAR-Processed Doppler-Delay Images

The received signals were processed at DSS-13 using the GSSR receiver (DCAR) and the images in Figures 14a–c generated using the SAOImageDS9 freeware application. In Figures 14a–c, Doppler is along the horizontal axis, and delay along the vertical axis.

An interesting approach for mitigating leakage is to shut off the transmitter via the “drive OFF” command but continue to collect data for one round-trip light-time (RTLTL) after the shutoff, which translates to about 2.6 seconds for the Earth-Moon link. This will eliminate the leakage altogether if the timing is correct, but it does limit the duration of the data set to RTLTL for any target. An example of this approach is shown in Figure 14a, where most of the multipath has indeed been eliminated with good (but not perfect) timing, using roughly 2.6 seconds of data. With more distant targets of interest, such as cislunar spacecraft or Near-Earth Asteroids (NEA), longer RTLTL will be possible: for interplanetary targets, the RTLTL will generally not be a limiting factor.

Figure 14b is a 10-second image obtained on DOY-037 over the DSS-26/28 link, clearly showing the target crater Tycho in the center. A two-transmitter, 10-second image was also obtained on DOY-037 over the DSS-13/26/28 link, showing two independent images of the same region with large relative delay but nominally aligned in Doppler in Figure 14c. This was achieved by offsetting the constant DSS-26 frequency by the predicted Doppler at the time when the 10-second data set was collected. The crater Tycho is visible in both images at the same Doppler frequency (along the horizontal axis) but with very different delays, corresponding to a large displacement in the vertical axis. Note the strong multipath band along the left edge of the image: This is a 10-second image, much longer than a lunar RTLTL; hence the leakage contribution could not be eliminated via the “drive OFF” approach. However, it was found that by timing the trajectory, high-quality Doppler-delay images can be obtained when the interference band is outside the Doppler frequencies covering

the Tycho region of the leakage signal as it drifts in Doppler due to the time-varying geometry between the DSS-13 transmitter and the DSS-28 receiver.

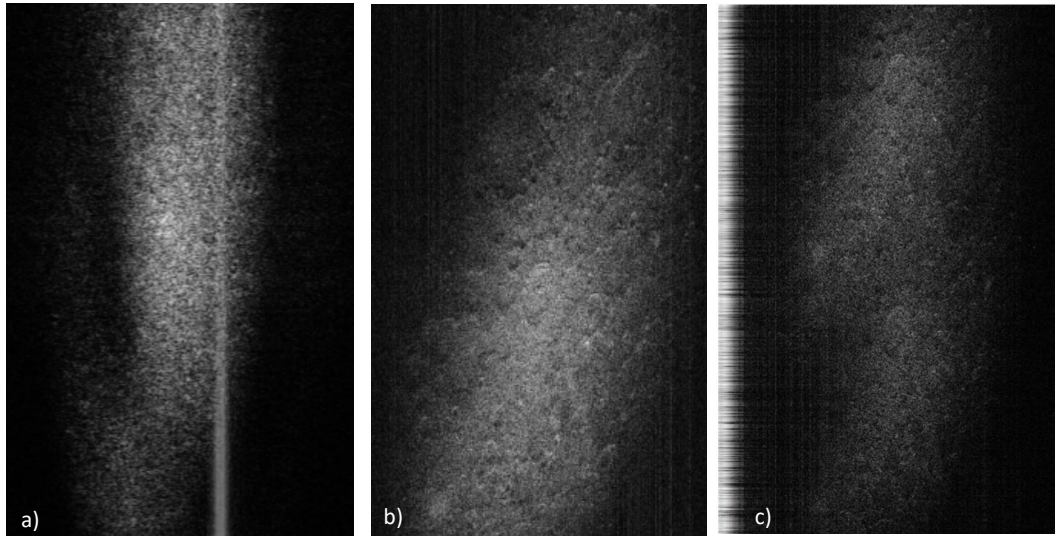


Figure 14. Doppler-delay images obtained with DCAR processing (Doppler axis horizontal, delay axis vertical):
a) DOY-035, DSS-13/28 link, single transmitter image of the Tycho region with $RTL = 2.6$ second data set, collected after transmitter “drive OFF” command; b) DOY-037, DSS-26/28 link, single-transmitter image, 10-second data set; c) DOY-037, DSS-13/26/28 link, two-transmitter dual image, 10 second data set.

VI. Upgrading the WFG for Predict-Driven Uplink Signals

Due to the incompatibility of the GSSR predict-files with the operational DSN linear ramping approach, it was necessary to transmit constant-frequency PN-11 code modulated signals out of each Apollo antenna, which in turn led to the development of custom predicts for compensating the DSS-13 uplink differentially to enable generating array fringes on the Moon, as described in Section 3. This approach in turn required the generation of differential predict files for the WFG and incorporating these files into the DSS-13 transmitter system for the differential uplink signals required for array fringe formation on the Moon.

A. Demonstrating Two-Antenna Doppler-Delay Images of Tycho

After the loss of two scheduled tracks in the spring and summer of 2020, one due to severe weather and the other due to restrictions on scheduling Apollo antennas before the Mars 2020 launch, a set of three consecutive tracks were finally scheduled on DOY-214/215/216 (August 1st, 2nd, 3rd) following successful launch of the Mars 2020 spacecraft on July 30th.

A day before the first track, two power supplies in the DSS-28 receiver failed, likely due to extreme temperatures at Goldstone, and the entire three-day campaign was in jeopardy. However, due to heroic efforts by the DSS-13 Group Supervisor Larry Snedeker and the DSS-13 staff, Jeff Lagrange and Tyler Tennyson, the DSS-28 receiver was repaired in one day and thereafter functioned flawlessly for the remaining two tracks.

The WFG was upgraded for Doppler and delay-compensated differential uplink transmission from DSS-13, and applied to the Doppler-delay image formation of the Tycho region. Since the initial delay offset is due primarily to electronics and not to predictable geometry, it is not well known. Therefore, an initial two-antenna Doppler-delay image similar to Figure 14c was formed and displayed via the commercial freeware SAOImageDS9 application. The cursor in this application can be used to search the image on a pixel level, where the delay resolution is determined by the 200 kHz PN-11 code used in this experiment, and the delay difference input into the WFG to approximate the initial delay offset.

On the final day of these tracks, DOY-216, the DSS-13 transmitter was compensated for differential Doppler and delay, DSS-24 transmitted a fixed frequency 7150 MHz PN-11 code modulated signal, and the echoes received at DSS-28 were processed via frequency and delay predicts to generate the overlapping two-antenna images. The results of this final track are shown in Figure 15, where the first pair demonstrates 5-microsecond pixel-level delay alignment (corresponding to 200 kHz chip rate) that shows up as visually overlapped Tycho crater images with the initial delay offset applied; the next pair in Figure 15b show the same received signal without delay compensation, clearly demonstrating delay offset in the two images. Finally, the last two images in Figure 15c verify that the application of the coarse delay estimates are correct to roughly a single chip in delay by overlapping the two-antenna images formed by DSS-13 and DSS-24. These images were taken on DOY-216, just before the end of the track.

However, well-defined array fringes similar to those observed earlier with the short baseline (~265 m) Apollo Uplink Array, as shown in Figure 16, were not observed in these two-antenna images. Due to the much longer 12 km baseline between DSS-24 and DSS-13, the long-baseline fringes will be approximately 50 times narrower than the Apollo fringes, as shown by the drawing in Figure 16, forming approximately 30 array fringes over the

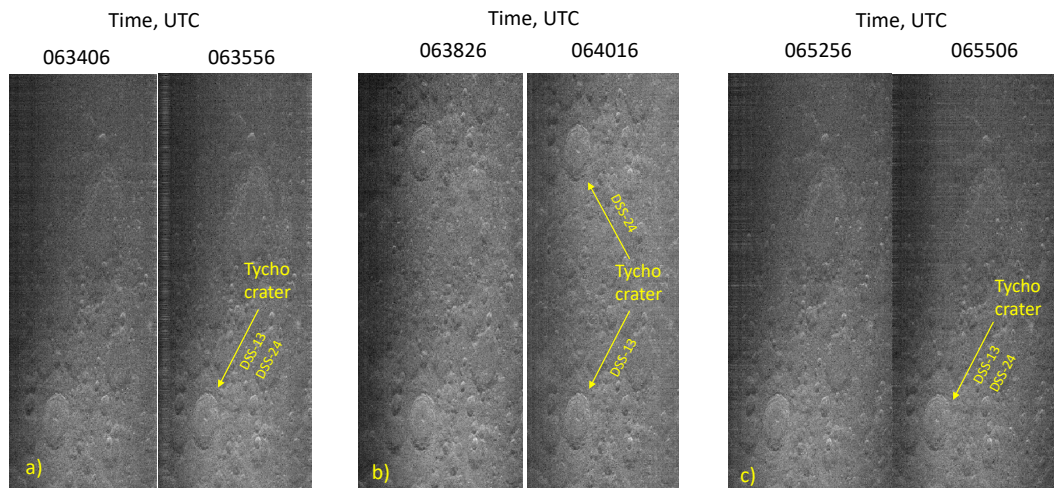


Figure 15. Sequence of two-antenna DSS-13/24 Doppler-delay images of the Tycho region on DOY-216: a) with coarse delay estimate applied; b) coarse delay estimate removed; c) verification step showing the merging of the images when the coarse delay estimate is reapplied and validating stability of the coarse delay estimate over 20 minutes.

Tycho crater. Generating such narrow array fringes requires fractional-chip delay alignment, which in turn requires additional upgrades to the WFG that will be implemented and tested in future experiments.

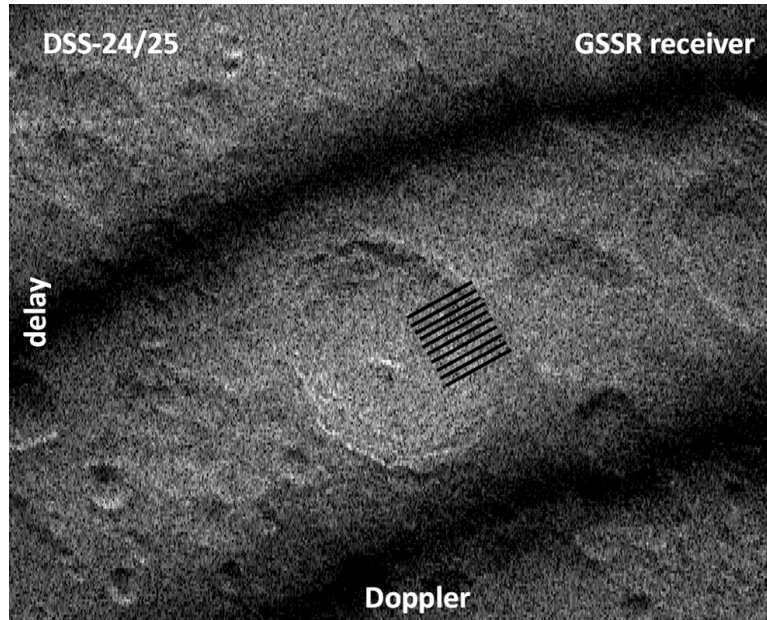


Figure 16. High-resolution Doppler-delay image of the Tycho region obtained with the DSS-24/25 Uplink Array in 2012, showing the spacing of the array fringes as well as a drawing of the expected spacing of the long-baseline fringes under similar conditions.

VII. Summary and Conclusions

The operational medium-power klystrons used by the DSN's 34 m antennas have proven to be reliable in the past; hence the proposed Uplink Array Radar will provide a useful backup to the current GSSR, as well as a potential ultra-high EIRP radar transmitter concept for future GSSR and DSN deep-space applications. The ultra-high EIRP concepts demonstrated in this effort can be automated for future infusion into the DSN as a low-risk Uplink Array Radar alternative to the current monolithic 70 meter ultra-high-power klystron approach.

In order to form array fringes on the Moon, the waveforms from the two transmitter stations must arrive at the target coherently with much less than half of the PN-11 code chip difference. The incompatibility of DSN predicts and sample-level GSSR predicts made it necessary to operate the Apollo antennas with constant carrier frequency; hence custom differential predicts were generated to pre-compensate the DSS-13 uplink signal such that the carrier frequencies were identical at the Moon. The sum of geometric and electronic delays was estimated by measuring the initial delay displacement of reference pixels in the displaced two-antenna Doppler-delay images, and this delay was applied to generate the overlapped two-antenna images shown in Figure 15. However, the formation of array fringes will require more precise delay compensation, which is the subject of follow-on development and experiments currently being planned for the next phase of the Uplink Array Radar development effort.

Acknowledgments

The authors would like to thank the Venus site Group Supervisor Lawrence Snedeker and staff, Jeffrey Lagrange and Travis Tennyson, for their invaluable help in carrying out the Goldstone tracks at DSS-13 and fixing the equipment on several occasions under conditions of extreme heat in the Mojave Desert.

References

- [1] V. Vilnrotter, D. Lee, T. Cornish, P. Tsao, L. Paal, V. Jamnejad, "Uplink array concept demonstration with the EPOXI spacecraft," *Proceedings of the IEEE Aerospace Conference*, Big Sky, Montana, March 2009.
- [2] V. Vilnrotter, P. Tsao, D. Lee, T. Cornish, L. Jao, M. Slade, "Planetary radar imaging with the Deep-Space Network's 34 meter Uplink Array," *Proceedings of the IEEE Aerospace Conference*, Big Sky, Montana, March 2011.
- [3] P. Tsao, V. Vilnrotter, V. Jamnejad, "Pointing-vector and velocity based frequency predicts for deep-space uplink array applications," *Proceedings of IEEE Aerospace Conference*, Big Sky, Montana, March 2009.
- [4] R. LaBelle, C. Buu, "Uplink and Downlink Electronics Upgrades for the NASA Deep Space Network Aperture Enhancement (DAE) Project," SpaceOps 2014 Conference, Pasadena, California, 5-9 May 2014.